buildings

MDPI

Article

Influence of Varying Curing Temperatures on the Mechanical and Durability-Related Performance of Multi-SCM Blended High-Strength Self-Compacting Concrete

Ibrahim M. Degani *, Riccardo Maddalena and Sivakumar Kulasegaram

School of Engineering, Cardiff University, Cardiff CF24 3AA, UK; maddalenar@cardiff.ac.uk (R.M.); kulasegarams@cardiff.ac.uk (S.K.)
* Correspondence: deganiim@cardiff.ac.uk

Abstract

Self-compacting concrete (SCC) offers major advantages in construction; however, its high paste content makes its performance highly sensitive to curing temperature and binder composition. This study evaluates the mechanical and durability behaviour of high-strength SCC incorporating silica fume (SF), metakaolin (MK), fly ash (FA), and a quaternary blend of these materials under different curing temperatures. The mixtures were cured at 10 °C, 20 °C, 35 °C, and 50 °C, and their compressive strength, sorptivity, bulk electrical resistivity, and length change were monitored up to 90 days. The results indicate that elevated curing temperatures significantly enhance early-age strength and reduce sorptivity and electrical conductivity, particularly in mixtures containing SF and MK, due to accelerated hydration and pore refinement. However, these conditions also led to increased length change, indicating greater deformation at both early and later ages. In contrast, curing at 10 °C reduced early strength but consistently improved long-term durability performance, especially in FA-containing mixtures, by promoting gradual hydration and reduced shrinkage. The quaternary blend exhibited balanced behaviour across all temperature regimes, achieving improved early strength while maintaining favourable long-term durability indicators. The innovation of this study lies in the integrated assessment of mechanical performance, transport properties, and dimensional stability of SCC incorporating multi-SCM systems under a wide range of curing temperatures, providing new insights into achieving stable and durable SCC performance under variable thermal conditions.

Keywords: self-compacting; temperature; sorptivity; electrical resistivity; shrinkage

Academic Editor: Cedric Payan

Received: 29 January 2026
Revised: 11 February 2026
Accepted: 13 February 2026
Published: 25 February 2026

1. Introduction

Over the past four decades, self-compacting concrete (SCC) has emerged as a significant advancement in concrete technology, offering numerous advantages over conventional concrete [1,2]. SCC is characterised by its ability to flow freely through densely reinforced and complex architectural elements without segregation or bleeding, ensuring uniformity and structural integrity. Unlike traditional concrete, SCC achieves adequate compaction solely through its self-weight, eliminating the need for external vibration [1,3,4]. Furthermore, SCC improves construction efficiency, leading to substantial time saving and project optimization [5–9].

However, the high paste content required for the self-compacting behaviour of SCC introduces challenges that influence both performance and sustainability. High cement

content increases the heat of hydration, porosity, shrinkage, and creep, while also escalating material costs and environmental impact due to carbon emissions and raw material consumption [10–12]. From a durability perspective, the larger paste volume being more prone to volumetric changes than aggregates leads to reduced dimensional stability, increased water absorption, and a more porous microstructure [1,13–19]. These factors accelerate deterioration mechanisms such as chloride ingress, freeze-thaw damage, and reinforcement corrosion, especially in aggressive environments [19–24].

Temperature is another critical factor that influences the performance of SCC, particularly in relation to hydration rate and microstructure formation. Low curing temperatures slow hydration, initially reducing strength gain but eventually contributing to a denser, more refined pore network and improved long-term durability [25–30]. In contrast, high temperatures accelerate hydration and moisture loss, leading to greater capillary tension, early-age shrinkage, and internal stresses. This results in a heterogeneous pore structure, diminished dimensional stability, and increased susceptibility to microcracking and water permeability [31–36].

Supplementary Cementitious Materials (SCMs) can be used to address these issues. SCMs enhance the mechanical and durability properties of SCC by refining the microstructure, modifying hydration behaviour, and reducing overall paste content and environmental impact [9,37,38]. High-reactivity SCMs like silica fume (SF) and metakaolin (MK) improve strength and pore refinement, while low-reactivity SCMs such as fly ash (FA) and Ground Granulated Blast-furnace Slag (GGBS)help manage heat generation and mitigate shrinkage, especially under elevated curing temperatures [39–42]. Their performance is further influenced by environmental conditions, with high-reactivity SCMs suited to cold climates due to their ability to enhance early hydration, and low-reactivity ones providing better thermal performance and reduced shrinkage in hot environments, thereby maintaining microstructure [18,26,43,44].

Previous research has predominantly focused on the durability of conventional concrete, with limited investigation into its performance under varying curing temperatures. To the authors' knowledge, the long-term durability behaviour of self-compacting concrete (SCC), particularly when incorporating SCMs under different curing temperatures, remains largely unexplored. This study aims to address this research gap by evaluating the short- and long-term durability performance of high-strength SCC containing treated SCMs under controlled thermal conditions. The novelty of this research lies in its comprehensive assessment of SCC durability through multiple experimental approaches, including compressive strength testing, length change measurements, water absorption analysis, and chloride ion penetration tests. A reference SCC mixture was prepared using Portland cement as the sole binder, while modified mixtures incorporated 10% silica fume (SF), 10% metakaolin (MK), and fly ash (FA) at replacement levels of 20% and 40%, along with a quaternary blend consisting of 10% SF, 10% MK, and 30% FA. Specimens were subjected to water curing at temperatures of 10 °C, 20 °C, 35 °C, and 50 °C to assess their mechanical and physical performance across varying thermal conditions. The findings of this study offer critical insights into the durability characteristics of SCC in different curing environments, supporting its potential as a sustainable and high-performance material in modern construction applications.

2. Materials and Methods

2.1. Materials

In this study, Portland cement (PC) with a compressive strength grade of 52.5 MPa (CEM I 52.5 N) supplied by Blue Circle Cement, (Dunbar, UK), FA obtained from Tarmac Group, (Birmingham, UK), MK supplied by Imerys Minerals, (Paris, France), and SF

provided by Elkem Microsilica, (Svelgen, Norway) was utilized. The chemical composition of the Portland cement and other supplementary replacement materials is detailed in Table 1. Polycarboxylate ether polymer superplasticiser (SP) (MasterGlenium ACE 499) with a specific gravity of 1.07 supplied by BASF Construction Chemicals, (Trostberg, Germany) was incorporated to improve the mixes' workability. The aggregate used included crushed limestone coarse aggregate (CA) with a maximum gravel size of 10 mm and a specific gravity of 2.65, and natural river sand as the fine aggregate with a maximum particle size of 2 mm and a specific gravity of 2.55. About 30% of the river sand was substituted with a coarser limestone dust (LD) (crushed rock sand) fraction, which has a specific gravity of 2.6 and particle sizes ranging from 2.0 mm to 0.125 mm. All aggregates were sourced from Breedon's Wenvoe Quarry, South Wales, (Wenvoe, UK). Figure 1 illustrates the particle size distribution curves for both fine and coarse aggregates.

Table 1. Chemical composition and physical properties of the binder materials as provided by the suppliers.

Composition	SiO_2 %	Al_2O_3 %	Fe_2O_3 %	CaO %	K_2O %	Na_2O %	MgO %	SO_3 %	Specific Gravity
PC	19.69	4.32	2.85	63.04	0.74	0.16	2.17	3.12	3.15
SF	85	-	-	1	-	4	-	2	2.2
FA	53.10	20.64	8.93	6.12	2.17	1.68	1.79	1.93	2.4
MK	57	36.97	0.40	-	1.46	-	1.26	0.54	2.5

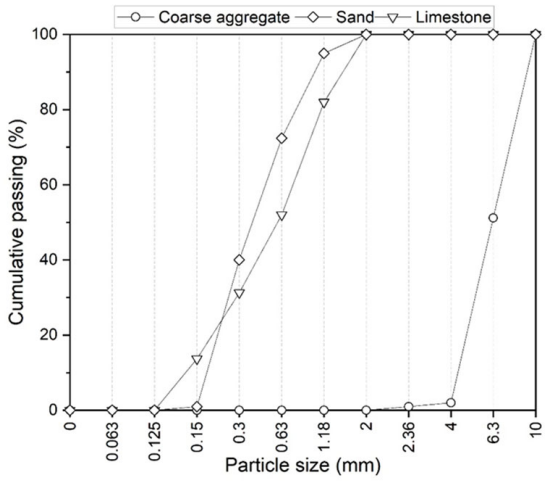

Figure 1. Particle size distribution curves of aggregate.

2.2. Mix Proportion

To evaluate the fresh, mechanical, and durability properties of SCC, six mixes were designed and casted. All mixtures were designed with a water-cement (W/C) ratio of 0.40 to meet the target compressive strength of 70 MPa at 28 days. FA and SF were incorporated as partial substitutes for PC at replacement rates of 20% and 40% for FA and 10% for SF, respectively. A quaternary blend combining 10% SF, 10% MK, and 30% FA was also formulated, achieving a total cement replacement of 50% by weight. Due to the high-water demand of SF owing to its fine texture, adjustments were made to the volume of SP in the SF-blended mixes to ensure their self-compacting properties. On the other hand, due to the spherical particle effect of FA, which improves flowability, and because its particles are larger and less reactive compared to SF, reductions were made to both water and SP volumes in the FA mixes. This adjustment ensures improved workability and

fluidity, maintaining the self-compacting characteristics of the concrete. Details of the mixed proportions can be found in Table 2. The concrete mixtures were designated using the format X–Y, where 'X' indicates the type of SCMs incorporated and 'Y' refers to the proportion of cement replaced. The quaternary blend was identified as Q–50, representing a total cement substitution of 50%. For comparative purposes, a control mix consisting entirely of Portland cement was also included and designated as PC–100.

Table 2. Proportions of constituent materials used in the studied SCC mixes, expressed in kg/m^3.

Mix ID	Water	Cementitious Material				SP	Aggregates		
		PC	SF	FA	MK		Fine		Coarse
							Sand	Limestone	
PC-100	205.6	514.1	-	-	-	3.3	525	225	833.0
SF-10	205.6	462.6	51.4	-	-	5.4	525	225	820.5
MK-10	205.6	462.6	-	-	51.4	5	525	225	810
FA-20	205.6	411.2	-	102.7	-	3.5	506.3	217	796
FA-40	205.6	308.4	-	205.6	-	3	515.3	220.8	796.9
Q-50	205.6	257.05	51.5	154.2	51.5	4	504.9	216.3	789.3

Note: PC = Portland cement; SF = Silica fume; FA = Fly ash; MK = Metakaolin; SP = Superplasticiser.

2.3. Sample Preparation

The composition of SCC was designed and prepared following a systematic mixing sequence to ensure homogeneity and reproducibility [8,30]. Initially, coarse aggregate (previously oven-dried) were introduced into the mixer and blended for 45 s. This was followed by the addition of Portland cement (PC), which was mixed with the coarse aggregate for another 45 s. Subsequently, fine aggregate and limestone dust (also oven-dried) were added simultaneously and mixed for 1 minute to ensure a uniform distribution of materials. SCMs were then incorporated and mixed for a 1 additional minute. The SP, previously dissolved in water, was added in two stages, with the remaining portion introduced gradually. The final mixing phase continued for 4 additional minutes, resulting in a total mixing time of 7.5 min.

Prior to casting, fresh concrete properties were evaluated to ensure the compliance of SCC with the required performance criteria. The slump flow test was conducted to assess flowability, while the J-ring test was performed to determine passing ability, in accordance with SCC standards [45].

2.4. Casting, Curing, and Testing Procedures

After ensuring that the experimental SCC mixtures met the required flowability performance criteria, the concrete was cast into moulds of various sizes and shapes, depending on the respective test requirements. The moulded samples were covered with polyethylene sheets and cured in water tanks at temperatures of 10 °C, 20 °C, 35 °C, and 50 °C, respectively, to evaluate the influence of temperature on the mechanical and durability properties of SCC. After 24 h, the specimens were demoulded and returned to the curing tanks, where they remained until testing.

For the compressive strength test, cubic specimens (100 × 100 × 100 mm) were prepared following BS EN 12390-3:2023 [46,47]. The specimens were cured and tested at 3, 28, and 90 days. To assess length change behaviour, prismatic specimens (75 × 75 × 280 mm) were cast and tested based on BS EN 12350-16 2019 [48], with measurements recorded at 1, 3, 7, 14, 28, 56, and 90 days, using a length comparator device and a reference rod.

A bulk electrical resistivity test was conducted to indirectly assess concrete resistance to chloride ions penetration [49]. For this purpose, cylindrical specimens (100 mm diameter × 200 mm height) were cast and tested at 1, 3, 7, 14, 28, 56, and 90 days.

Additionally, water absorption rate was determined following ASTM C1585 [50], for which cylindrical specimens (100 mm diameter × 50 mm height) were prepared. Sorptivity values were obtained from the average of three specimens, with measurements performed at 3, 28, and 90 days.

The reported results for each test represent the average of at least three samples per measurement. If the standard deviation exceeded 10%, an additional sample was tested to enhance the accuracy of the reported values.

3. Results and Discussion

3.1. Fresh State

Table 3 presents the results of the fresh property tests, including slump flow, (T_{50}) time, and J-ring flow spread, for all concrete mixes. These tests are widely adopted to assess SCC characteristics in accordance with EFNARC guidelines [45].

Table 3. Fresh state test results of concrete mixes.

Mix ID	Slump Flow Test Spread (mm)	T_{50} (s)	J-Ring Flow Test Spread (mm)	ΔD = D_slump − D_(J-ring) (mm)
PC-100	630	1.82	600	30
SF-10	650	2.05	610	40
MK-10	660	2.1	615	45
FA-20	700	1.6	680	20
FA-40	710	1.1	695	15
Q-50	660	1.7	640	20

SCC is characterised by its filling ability, passing ability, and segregation resistance [1]. As shown in the table, all mixes achieved a slump flow spread within the acceptable range of 550–850 mm, indicating adequate flowability in line with standards. The (T_{50}) values for all mixes also fell within the expected limits, confirming appropriate viscosity and flow rate.

The J-ring test results, used to assess passing ability, showed that none of the mixes exhibited blockage behaviour. The differences between slump flow and J-ring flow spreads (ΔD values) were all below 45 mm, which is within the acceptable range for SCC and indicates good passing ability without significant obstruction from simulated reinforcement [51]. Visual observation during testing further confirmed the absence of segregation in all mixes.

The inclusion of SCMs had a notable effect on workability. Mixes containing silica fume (SF) and metakaolin (MK) demonstrated slightly reduced spread and higher (T_{50}) times, attributed to their fine particle size and high surface area, which increase water demand. As a result, these mixes required higher superplasticiser dosages to meet SCC flowability standard [52–55]. This observation aligns with previous research indicating that ultrafine materials tend to reduce free water availability and thus reduce workability [56,57].

In contrast, mixes incorporating FA, particularly at 20% and 40% replacement levels, exhibited the highest slump flow values and lowest (T_{50}) times. This improvement in flow is attributed to the spherical particle shape and lower density of FA, which enhances the lubrication effect and reduces inter-particle friction [58,59]. Consequently, lower dosages of superplasticiser were needed to achieve SCC properties in FA-based mixtures. The Q-50 mix, which included a combination of FA, SF, and MK, demonstrated balanced fresh performance, showing satisfactory flowability and passing ability [60,61].

3.2. Mechanical Performance

Compressive Strength

Figure 2 illustrates the development of compressive strength under different curing temperatures, highlighting the strong interaction between binder composition, hydration kinetics, and pozzolanic activity. As expected, compressive strength increased with age for all SCC mixtures; however, curing temperature exerted a decisive influence on both early-age and long-term performance. At 3 days, elevated curing at 50 °C significantly accelerated early hydration reactions. The PC mixture achieved a compressive strength of 48.2 MPa when cured at 20 °C, which increased to 58.1 MPa at 50 °C, corresponding to an increase of approximately 20%. This enhancement is consistent with the thermal activation of clinker hydration and accelerated early C–S–H formation reported by [62], who linked higher curing temperatures to accelerated clinker hydration and rapid early strength gain. The effect was more pronounced in mixtures incorporating highly reactive SCMs. SF-10 and MK-10 reached early-age strengths of 50.1 MPa and 47.8 MPa at 20 °C, which increased to 67.1 MPa and 64.2 MPa at 50 °C, representing gains of 39% and 33%, respectively. These improvements are attributed to their ultrafine particle size and high pozzolanic reactivity, which promote enhanced nucleation, rapid hydrate precipitation, and early matrix densification, in agreement with [38,42], who attributed similar strength gains to increased nucleation sites and accelerated secondary hydrate formation under elevated temperatures. The Q-50 mixture also benefited from elevated curing temperature, achieving an early strength of 49.4 MPa at 50 °C compared with 38.5 MPa at 20 °C, although the magnitude of improvement was lower than that observed in SF- and MK-based systems. This reflects complementary interactions between rapidly reacting SCMs (SF and MK) and the slower activation of FA. In contrast, FA-based mixtures exhibited delayed early-age strength development. At 35 °C, both FA-20 and FA-40 recorded compressive strengths (46.3 MPa and 35 MPa) lower than that of PC cured at 20 °C, reflecting the limited reactivity of FA at moderate temperatures. However, at 50 °C, FA-20 reached 55.6 MPa, surpassing the PC strength at 20 °C, demonstrating that FA requires higher thermal energy to achieve meaningful early hydration activity, as previously reported by [58].

Under cold curing (10 °C), all mixes exhibited reduced early strength due to a much slower hydration rate. The decline was most severe in the FA-rich mixes. Even SF-10 and MK-10, despite their high reactivity, showed notable reductions, indicating that low temperatures inhibit both clinker hydration and pozzolanic reactions [38,62–64].

Long-term behaviour at 90 days revealed distinct trends. The PC mixture cured at 50 °C reached a compressive strength of 65.7 MPa, which was 13.7% lower than that of PC cured at 20 °C (83.3 MPa), confirming the crossover effect described by [65], whereby rapid early hydration forms dense outer layers that restrict subsequent hydration dissolution and limit later-age strength development despite high early reaction rates. Similar reductions in long-term strength under hot curing have also been reported by [30,62]. In contrast, SF-10 and MK-10 cured at 50 °C achieved long-term strengths of 74.4 MPa and 70.9 MPa, comparable to PC cured at 20 °C and substantially higher than PC cured at 50 °C. This indicates that sustained pozzolanic activity and continued microstructural densification in these systems effectively counteracted the pore coarsening typically associated with high-temperature curing, consistent with the long-term behaviour of reactive SCMs reported by [43]. FA-20 and FA-40 also benefited from elevated temperatures at later ages, reaching strengths of 71.1 MPa and 70.4 MPa, respectively, exceeding PC cured at 50 °C yet remaining slightly below PC cured at 20 °C. These results highlight the slow yet continuous contribution of FA to strength development when thermally activated, as elevated temperatures enhance FA dissolution and secondary C–S–H formation over extended curing periods, as observed by [1,66].

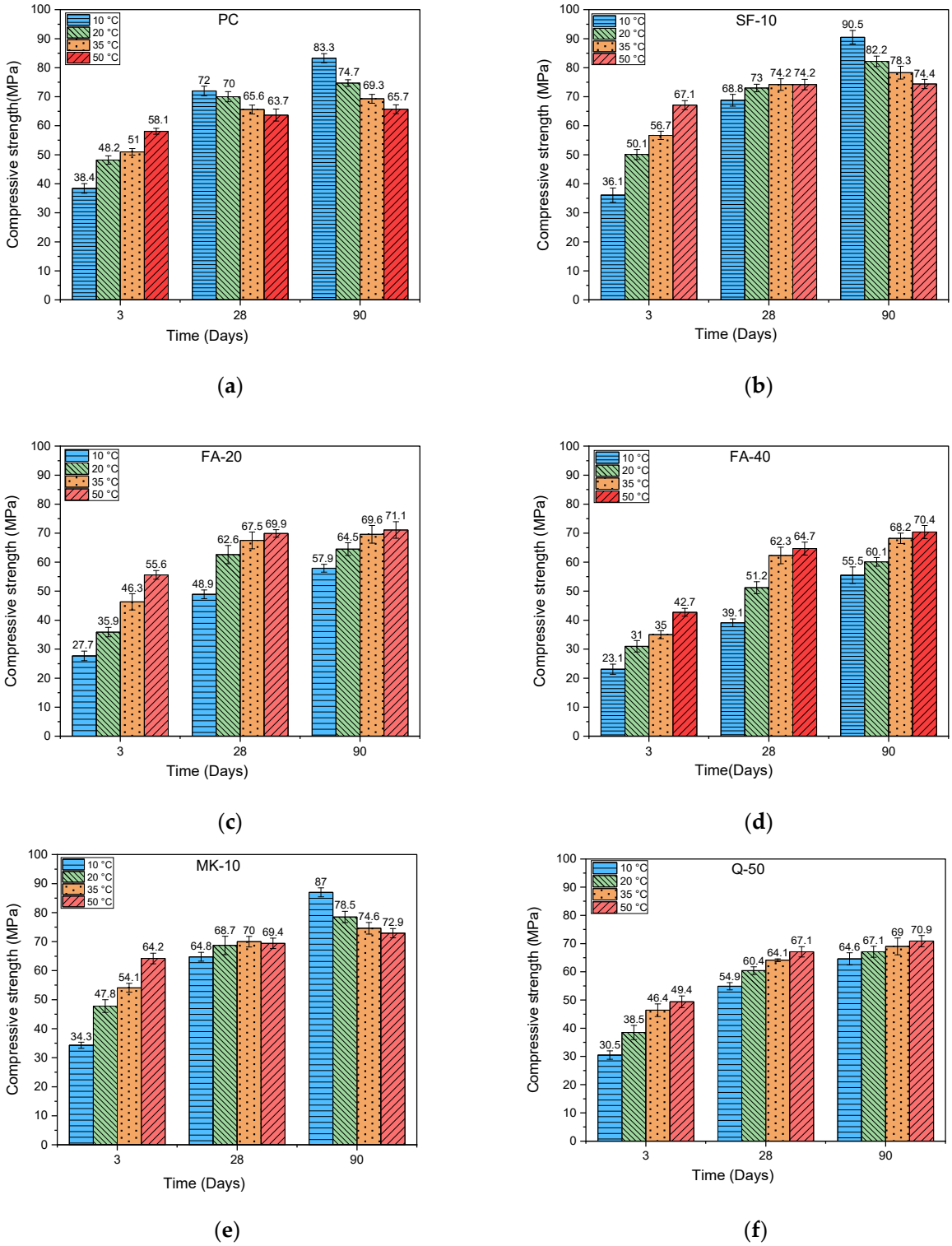

Figure 2. Compressive strength results: (**a**) PC mix, (**b**) SF-10 mix, (**c**) FA-20 mix, (**d**)FA-40 mix, (**e**) MK-10 mix, and (**f**) Q-50 mix.

Under cold curing at 10 °C, strength development was gradual yet persistent. At 90 days, the SF-10 and MK-10 mixtures achieved compressive strengths of 90.5 MPa and 87 MPa, respectively, exceeding the strength of the PC mixture cured at 20 °C (74.7 MPa) by 21% and 16.9%. This behaviour indicates that the pozzolanic reactions of SF and MK remain active even at low temperatures when sufficient curing time is provided, leading to progressive microstructural refinement and continued strength development, as reported

by [64,67]. Conversely, FA-20 and FA-40 recorded the lowest long-term strengths at 10 °C, reaching only 57.9 MPa and 55.5 MPa, respectively. This reduction is attributed to severely delayed FA activation caused by insufficient thermal energy for effective glass-phase dissolution at low temperatures, as noted by [63]. At 90 days, the compressive strength of the PC mixture cured at 10 °C (83.3 MPa) was approximately 11.5% greater than that of the mixture cured at 20 °C (74.7 MPa). This observation supports findings that slow hydration without early-age microcracking can preserve pore continuity and promote a denser and more stable long-term microstructure [62].

Overall, the compressive strength results demonstrate that curing temperature and SCM type strongly govern both early-age development and long-term performance, which in turn influence the durability-related properties discussed in the following sections.

3.3. Durability-Related Performance

3.3.1. Water Absorption

The sorptivity results presented in Figure 3 revealed clear temperature- and binder-dependent behaviours. At 3 days, curing at 50 °C substantially reduced sorptivity across all mixes by accelerating hydration and early pore densification. Reductions were especially pronounced in SF-10 and MK-10 (55–60%) compared to PC cured at 20 °C, reflecting their strong filler and nucleation effects, which [68] attributed to enhanced early C–S–H precipitation and refinement of capillary pores caused by ultrafine SCM particles. Q-50 also demonstrated reduced sorptivity, confirming the synergistic contributions of SF and MK. FA-20 and FA-40 showed moderate reductions, consistent with thermally enhanced yet still slow pozzolanic activation, as [69] reported that FA requires extended time or higher temperatures to significantly alter pore connectivity at early ages.

Cold curing increased early sorptivity in PC and FA mixes due to inhibited hydration and retained capillary porosity. However, SF-10 and MK-10 still exhibited noticeably lower sorptivity than PC at 20 °C, underscoring their ability to refine the pore network even under reduced temperature conditions, a behaviour linked by [62,63] to the combined influence of physical packing and the surface-controlled reactions of highly reactive SCMs at early ages [70].

At 90 days, SCM-containing mixtures consistently outperformed PC in lowering sorptivity under all curing temperatures. Under hot curing, reductions remained highest in SF-10, MK-10, and FA-rich mixes, reflecting continued pore densification through pozzolanic reactions, which [43,71] associated with long-term secondary hydrate formation and progressive reduction in pore connectivity. PC, however, exhibited increased sorptivity at 50 °C, likely due to coarser pore structure, associated with the crossover effect, as explicitly described by [65], where rapid early hydration under hot temperatures leads to long-term pore coarsening and increased transport properties [72]. Under cold curing, long-term sorptivity decreased substantially in all mixes, as slow yet sustained hydration generated a progressively denser microstructure [73].

These sorptivity trends reflect the underlying pore structure evolution, which is further examined through bulk electrical resistivity measurements.

The correlation presented in Figure 4 indicates a clear inverse trend between sorptivity and compressive strength for all mixes at both 3 and 90 days. This consistent behaviour suggests that mixes developing a denser and more refined pore structure exhibit simultaneously lower capillary suction and higher mechanical strength. Since sorptivity reflects the ease with which water is drawn through connected capillary pores, a reduction in pore volume and connectivity limits fluid absorb, resulting in reduced sorptivity values. The same improvement in the microstructure also enhances load-carrying capacity, which explains the corresponding increase in compressive strength. Although the mixes differ

in binder composition and hydration rate, the correlation maintains a similar form across all series, indicating that pore connectivity is a governing factor for both transport and mechanical performance. Early-age data (3 days) show greater scatter due to ongoing hydration, yet the overall trend remains visible. By 90 days, the relationships tighten, reflecting more stable and mature pore systems.

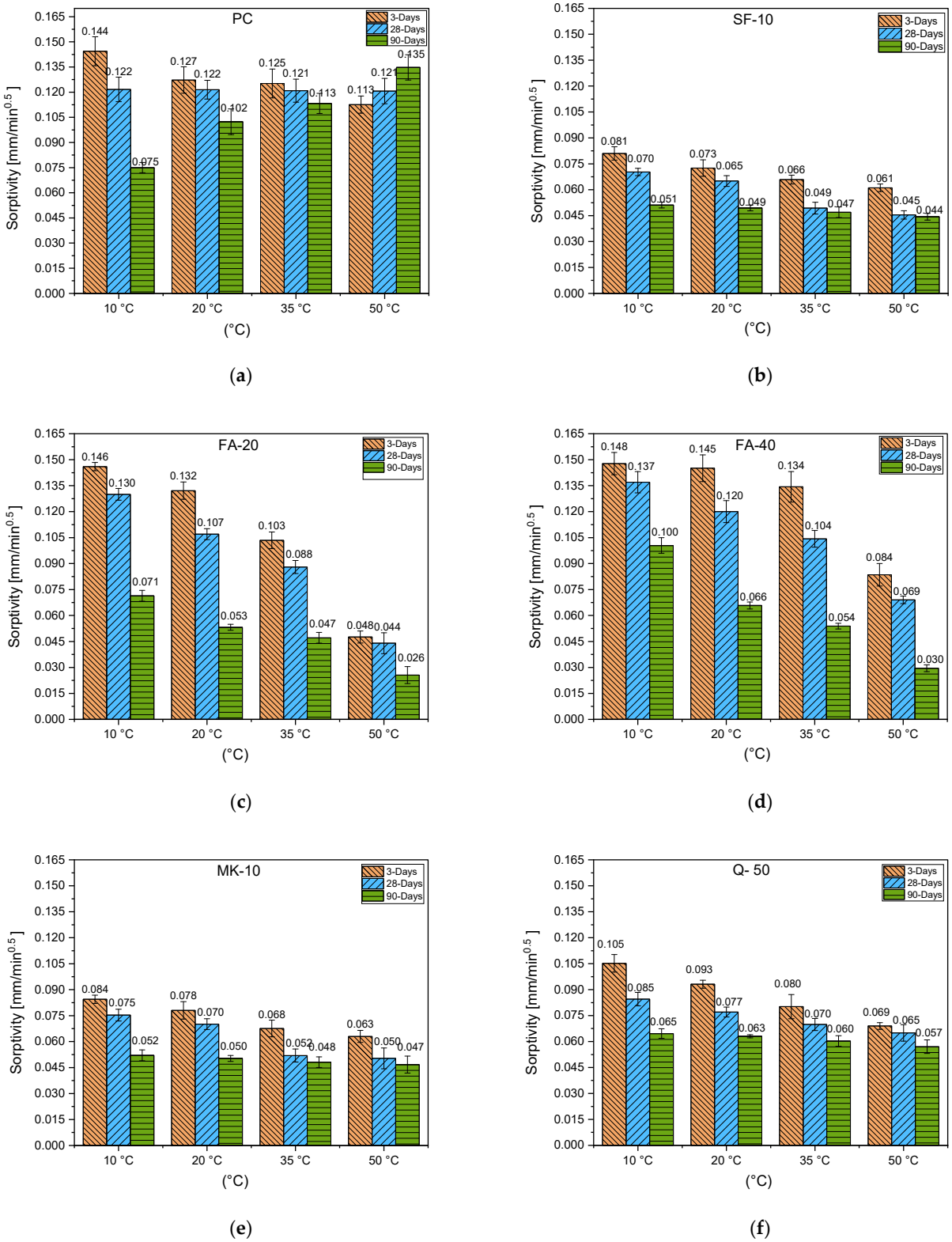

Figure 3. Sorptivity results: (**a**) PC mix, (**b**) SF-10 mix, (**c**) FA-20 mix, (**d**) FA-40 mix, (**e**) MK-10 mix, and (**f**) Q-50 mix.

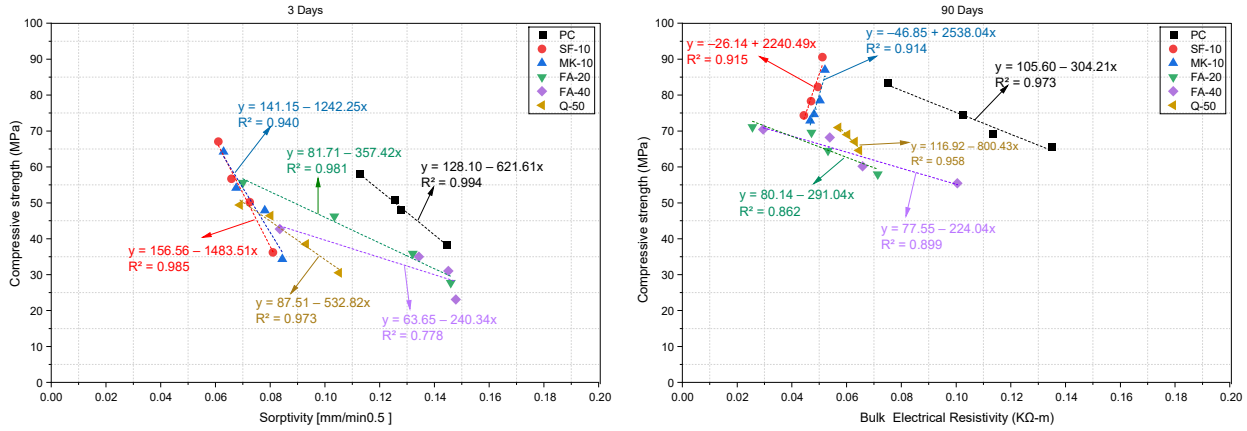

(**a**) (**b**)

Figure 4. Correlation between compressive strength and sorptivity: (**a**) correlation at 3 days, (**b**) correlation at 90 days.

The strong coupling between sorptivity and compressive strength suggests that sorptivity can serve as a practical durability indicator, complementing mechanical testing. Because sorptivity can be measured rapidly and non-destructively, it may offer a useful surrogate for assessing the microstructural quality of concrete and comparing different mix designs, particularly when durability-related testing is impractical or time-consuming.

3.3.2. Bulk Electrical Resistivity (BER)

Bulk electrical resistivity (BER), illustrated in Figure 5, exhibited behaviours consistent with the evolution of pore connectivity and moisture distribution, and its response to temperature closely aligned with the mechanisms identified in sorptivity. At 3 days, curing at 50 °C markedly increased BER in all mixes. The PC mixture recorded a value 144% higher than its BER at 20 °C, reflecting accelerated hydration and early densification of the pore network [62,74], which is consistent with the strong temperature-dependence of ionic transport and pore connectivity reported by [75]. The effect was far more clear in SCM-containing mixes: SF-10 and MK-10 achieved increases of 488% and 621% above their corresponding PC cured at 20 °C values, while the Q-50 blend reached 556% higher than PC at 20 °C. FA-20 and FA-40 also benefited substantially from thermal activation, attaining BER values 216–282% higher than those of PC cured at 20 °C. These large increases reaffirm the significant role of temperature in enhancing early microstructural densification through accelerated hydration and pozzolanic reactions [66], in agreement with [76], who observed sharp increases in the BER of concretes containing FA and SF when cured at high temperatures due to reduced capillary porosity and increased maturity.

Conversely, cold curing at 10 °C reduced early-age BER due to inhibited hydration and higher pore continuity [77], a trend also reported by [75], who observed consistently lower resistivity in specimens cured at 10 °C compared to those cured at higher temperatures. The PC mix measured 20% lower than its 20 °C value, and FA-based mixes showed reductions of approximately 30% below PC at 20 °C. Despite the low temperature, SF-10 and MK-10 maintained relatively elevated BER, registering 24–30% higher than PC cured at 20 °C, indicating that their fine particle size and partial pozzolanic activity continued to promote microstructural densification even under cold conditions [64,78], consistent with observations that highly reactive SCMs maintain higher BER through pore refinement mechanisms even when hydration kinetics are slowed. The Q-50 mixes remained comparable to PC at 20 °C, illustrating its moderated early response.

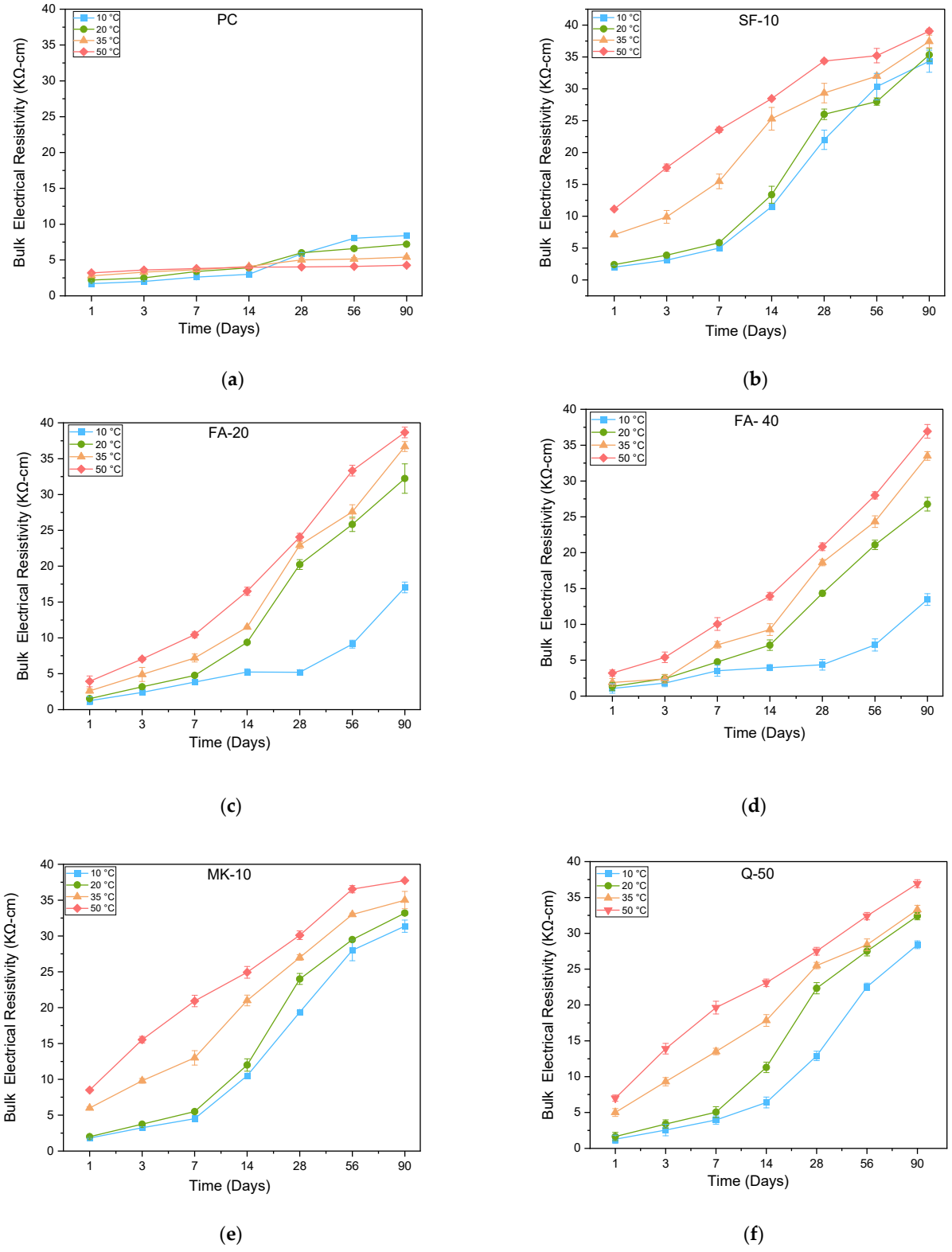

Figure 5. Bulk electrical resistivity results: (**a**) PC mix, (**b**) SF-10 mix, (**c**) FA-20 mix, (**d**) FA-40 mix, (**e**) MK-10 mix, and (**f**) Q-50 mix.

At 90 days, SCM-modified mixes cured at 50 °C exhibited the highest BER values, with SF-10, MK-10, FA-20, FA-40, and Q-50 achieving levels 412–442% higher than PC cured at 20 °C. These substantial long-term increases highlight the sustained contribution of pozzolanic activity to pore refinement under high temperatures [66,74,79], which is consistent with long-term BER trends reported by [76] for SCM-containing concretes cured

at 35–50 °C. In contrast, the PC mix cured at 50 °C declined to 60% lower than its 20 °C resistivity, confirming the crossover effect and the development of a coarser pore structure due to restricted later-age hydration [62,65], a behaviour also associated with the increased temperature sensitivity of BER in OPC systems, as described by [75].

Under cold curing (10 °C), long-term BER increased significantly across SCM mixes: SF-10 and MK-10 reached 335–357% higher than PC at 20 °C, and Q-50 reached 294% higher, while FA-20 and FA-40 achieved 136% and 87% higher, respectively. Even the PC mix ultimately surpassed its 20 °C performance. This behaviour demonstrates that extended, gradual hydration at low temperatures promotes progressive pore densification and reduced pore connectivity, as described by [62], and is consistent with the long-term BER recovery under cold curing reported by [76].

Together, the BER results corroborate the sorptivity findings and provide additional insight into the transport-related durability of SCC under different curing temperatures.

The relationship illustrated in Figure 6 shows a consistent interaction between compressive strength and BER across all SCC mixtures, reflecting the shared dependence of both parameters on pore structure development. At an early age, mixes exhibiting rapid hydration and initial microstructural improvement tend to demonstrate simultaneous increases in strength and resistivity. This behaviour indicates that early densification of the cementitious matrix enhances load-bearing capacity while also reducing ionic mobility by limiting pore connectivity. Such concurrent improvement suggests that hydration and pozzolanic reactions act synergistically during the initial curing period, producing a refined pore system that supports both mechanical and transport performance.

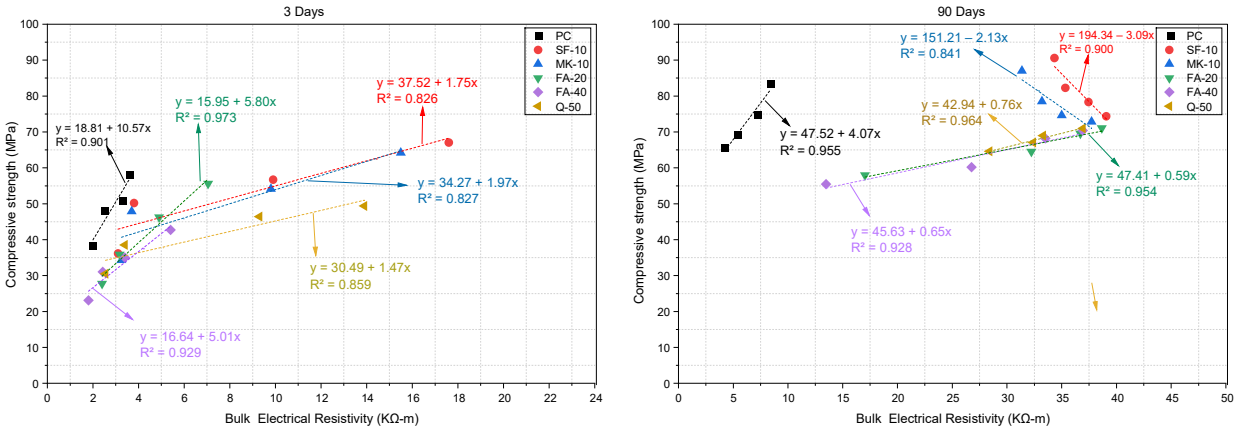

(**a**) (**b**)

Figure 6. Correlation between compressive strength and bulk electrical resistivity: (**a**) correlation at 3 days, (**b**) correlation at 90 days.

At later ages, the nature of this relationship becomes more sensitive to binder composition and curing conditions. Mixes dominated by continued hydration or gradually activated pozzolanic reactions maintain a direct correspondence between strength development and BER gains, reflecting ongoing pore improvement and progressive densification of the microstructure. In contrast, systems containing highly reactive SCMs under hot curing conditions may depart from this trend. Early accelerated reactions in these mixes can produce dense but less uniform matrices in which later hydration is restricted. Thermal effects, moisture loss, and microcracking may further disrupt pore continuity, leading to increased resistivity even when strength gain slows or stabilizes.

3.3.3. Length Change

Figure 7 illustrates the length-change development of SCC mixes under different curing temperatures, demonstrating that curing temperature and SCM composition significantly influence both early-age and long-term shrinkage. At early ages, when samples are effectively sealed, length change is governed primarily by autogenous shrinkage, caused by self-desiccation during hydration. At later ages, cumulative length change increasingly reflects drying-related shrinkage, associated with moisture redistribution and loss. Similar distinctions between early autogenous and later drying-controlled shrinkage have been reported by [80]. At 3 days, curing at 50 °C produced the highest early-age shrinkage in all mixes, indicating intensified autogenous shrinkage. The PC mix exhibited a 102% increase relative to curing at 20 °C, confirming that accelerated hydration rapidly consumed internal pore water and generated high capillary tension [62]. This behaviour is consistent with findings by [36], who attributed increased early-age shrinkage under high temperatures to rapid self-desiccation driven by accelerated hydration kinetics.

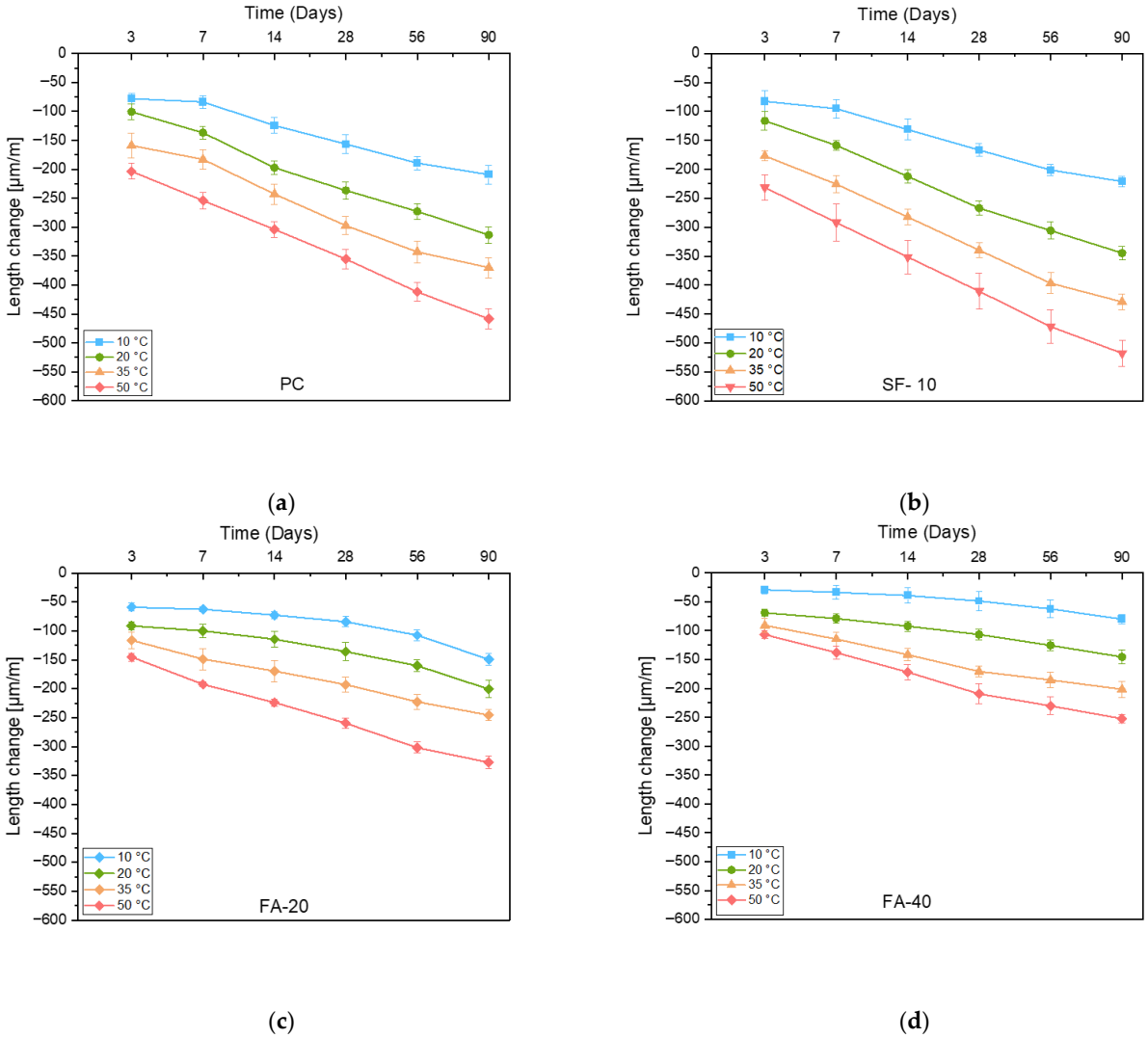

Figure 7. *Cont.*

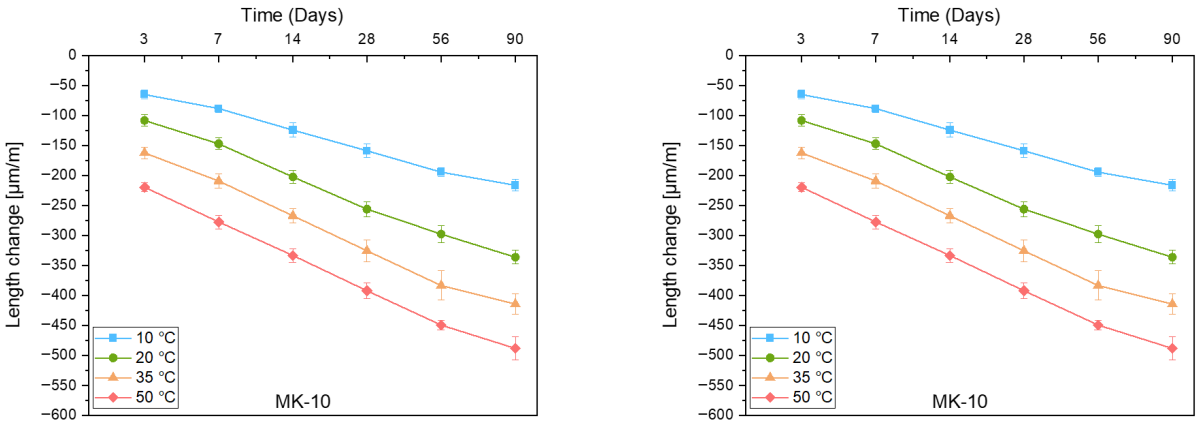

(**e**) (**f**)

Figure 7. Length change results: (**a**) PC mix, (**b**) SF-10 mix, (**c**) FA-20 mix, (**d**) FA-40 mix, (**e**) MK-10 mix, and (**f**) Q-50 mix.

The effect was more obvious in SCM-modified mixes. SF-10 and MK-10 exhibited increases of 130% and 119%, respectively, reflecting their ultrafine particle size and strong nucleation capacity, which intensified early hydrate formation and self-desiccation. Similar increases in early autogenous shrinkage for SF- and MK-modified systems cured at high temperatures were reported by [81], who linked this behaviour to rapid pore refinement and increased internal water demand. The Q-50 mix showed a more moderate increase (80%), indicating that the combined presence of rapidly reacting SCMs (SF and MK) and FA moderated early hydration intensity. In contrast, FA-20 and FA-40 showed the smallest early-age increases (44% and 6%, respectively), consistent with the slow pozzolanic activation and low early-age water demand of FA. Similar reductions in early autogenous shrinkage due to FA incorporation were reported by [82].

Under cold curing at 10 °C, early-age shrinkage was substantially reduced for all mixes, confirming the suppression of autogenous shrinkage at low temperatures. The PC mix showed a 22.5% reduction, while FA-20 and FA-40 exhibited the largest reductions (41% and 71%), reflecting the very low early reactivity of FA at lower temperatures. Comparable reductions in early autogenous shrinkage under low curing temperatures were also reported by [80].

At 90 days, the influence of curing temperature on drying shrinkage became more evident. Under curing at 50 °C, most mixes exhibited increased cumulative shrinkage compared to those cured at 20 °C. The PC mix increased by 46%, while SF-10 and MK-10 increased by 56% and 65%, respectively, indicating that high temperatures enhanced long-term moisture loss through sustained hydration and pore refinement. Similar long-term increases were reported by [62,83]. In contrast, FA-20 showed only a marginal increase (4%), while FA-40 exhibited a reduction of 19%, confirming that the slower and more uniform hydration of FA effectively limited long-term drying shrinkage, consistent with observations by [82,84]. Cold curing at 10 °C consistently produced the lowest long-term shrinkage across all mixes, indicating that reduced temperatures limited drying rates and preserved internal relative humidity, thereby improving long-term length change [80].

4. Conclusions

This study explored the influence of curing temperature on the mechanical and durability performance of high-strength SCC incorporating SCMs, including SF, MK, FA, and quaternary blend. The key findings are as follows:

- The inclusion of high-reactivity SCMs such as SF and MK reduced the workability of SCC due to their high surface area and water demand, requiring increased superplasticizer dosage. In contrast, FA enhanced workability by promoting better flowability through its spherical particle shape and lower water demand.
- Durability-related indicators such as sorptivity and electrical resistivity reflected the interplay between SCM type and curing regime. High temperatures were due to rapid pore refinement in SF and MK mixes. However, low temperatures resulted in higher early-age sorptivity and lower resistivity but allowed gradual long-term improvement, particularly in FA and Q-50 mixes.
- Length change was significantly influenced by curing temperature and SCM type. High temperatures accelerated hydration, causing early shrinkage in SF and MK mixes due to rapid internal water loss. In contrast, low temperature curing reduced early shrinkage in all mixes by slowing hydration and limiting self-desiccation. FA mixes showed minimal early shrinkage across all conditions, while the quaternary blend (Q-50) exhibited controlled and gradual shrinkage, combining early matrix densification with long-term stability.
- The correlations between compressive strength and durability metrics (sorptivity and bulk electrical resistivity) were generally strong, particularly at later ages, confirming the interconnected development of mechanical and durability properties. This reinforces the importance of incorporating SCMs with varied reactivity profiles to enhance overall performance.

Author Contributions: Writing—original draft, investigation, formal analysis, data curation, conceptualization, I.M.D.; review & editing, supervision, and methodology, R.M.; writing—editing, supervision, project administration, and methodology, S.K. All authors have read and agreed to the published version of the manuscript.

Funding: This research received no external funding.

Data Availability Statement: The datasets generated and analysed during the present study are publicly available in the Figshare repository at: https://doi.org/10.6084/m9.figshare.31384522. The repository includes the full set of raw experimental data corresponding to the Compressive strength, bulk electrical resistivity, and length change tests described in this study.

Conflicts of Interest: The author declares no conflicts of interest.

References

1. Khatib, J.M. Performance of self-compacting concrete containing fly ash. *Constr. Build. Mater.* **2008**, *22*, 1963–1971. [CrossRef]
2. Long, G.; Gao, Y.; Xie, Y. Designing more sustainable and greener self-compacting concrete. *Constr. Build. Mater.* **2015**, *84*, 301–306. [CrossRef]
3. Okamura, H.; Ozawa, K. Self-compacting high performance concrete. *Struct. Eng. Int. J. Int. Assoc. Bridge Struct. Eng. (IABSE)* **1996**, *6*, 269–270. [CrossRef]
4. Soleymani Ashtiani, M.; Scott, A.N.; Dhakal, R.P. Mechanical and fresh properties of high-strength self-compacting concrete containing class C fly ash. *Constr. Build. Mater.* **2013**, *47*, 1217–1224. [CrossRef]
5. Zhu, W.; Gibbs, J.C.; Bartos, P.J.M. Uniformity of in situ properties of self-compacting concrete in full-scale structural elements. *Cem. Concr. Compos.* **2001**, *23*, 57–64. [CrossRef]
6. Ma, A.; Abba, S.I.; Nuruddeen, M.M. Self-Compacting Concrete—A Review. *Int. J. Innov. Technol. Explor. Eng.* **2017**, *6*, 1–7.
7. Mosafer, M.; Khodabakhshian, A.; Ghalehnovi, M. Case Studies in Construction Materials Optimizing the mechanical properties of sustainable self-compacting concrete contains industrial by-products by using Taguchi and Grey-Taguchi methods. *Case Stud. Constr. Mater.* **2025**, *22*, e04692. [CrossRef]
8. Alshahrani, A.; Cui, T.; Almutlaqah, A.; Kulasegaram, S. Designing sustainable high-strength self-compacting concrete with high content of supplementary cementitious materials. *Eur. J. Environ. Civ. Eng.* **2024**, *28*, 1830–1849. [CrossRef]
9. Gupta, N.; Siddique, R.; Belarbi, R. Sustainable and Greener Self-Compacting Concrete incorporating Industrial By-Products: A Review. *J. Clean. Prod.* **2021**, *284*, 124803. [CrossRef]

10. Okamura, H.; Ouchi, M. Self Compacting Concrete—Research paper. *J. Adv. Concr. Technol.* **2003**, *1*, 5–15. [CrossRef]
11. Ouldkhaoua, Y.; Benabed, B.; Abousnina, R.; Kadri, E.H.; Khatib, J. Effect of using metakaolin as supplementary cementitious material and recycled CRT funnel glass as fine aggregate on the durability of green self-compacting concrete. *Constr. Build. Mater.* **2020**, *235*, 117802. [CrossRef]
12. Kolias, S.; Georgiou, C. The effect of paste volume and of water content on the strength and water absorption of concrete. *Cem. Concr. Compos.* **2005**, *27*, 211–216. [CrossRef]
13. Klemczak, B.; Gołaszewski, J.; Smolana, A.; Gołaszewska, M.; Cygan, G. Shrinkage behaviour of self-compacting concrete with a high volume of fly ash and slag experimental tests and analytical assessment. *Constr. Build. Mater.* **2023**, *400*, 132608. [CrossRef]
14. Ndahirwa, D.; Zmamou, H.; Lenormand, H.; Leblanc, N. The role of supplementary cementitious materials in hydration, durability and shrinkage of cement-based materials, their environmental and economic benefits: A review. *Clean. Mater.* **2022**, *5*, 100123. [CrossRef]
15. Rozière, E.; Granger, S.; Turcry, P.; Loukili, A. Influence of paste volume on shrinkage cracking and fracture properties of self-compacting concrete. *Cem. Concr. Compos.* **2007**, *29*, 626–636. [CrossRef]
16. Hwang, S.D.; Khayat, K.H. Effect of mixture composition on restrained shrinkage cracking of self-consolidating concrete used in repair. *ACI Mater. J.* **2008**, *105*, 499–509. [CrossRef]
17. Leemann, A.; Lura, P.; Loser, R. Shrinkage and creep of SCC—The influence of paste volume and binder composition. *Constr. Build. Mater.* **2011**, *25*, 2283–2289. [CrossRef]
18. Kalyana Chakravarthy, P.R.; Namratha, K. Strength and durability properties of high strength self compacting concrete. *Mater. Today Proc.* **2022**, *69*, 896–900. [CrossRef]
19. Shaikh, F.U.A.; Supit, S.W.M. Chloride induced corrosion durability of high volume fly ash concretes containing nano particles. *Constr. Build. Mater.* **2015**, *99*, 208–225. [CrossRef]
20. Wang, Y.; Cao, Y.; Zhang, P.; Ma, Y.; Zhao, T.; Wang, H.; Zhang, Z. Water absorption and chloride diffusivity of concrete under the coupling effect of uniaxial compressive load and freeze–thaw cycles. *Constr. Build. Mater.* **2019**, *209*, 566–576. [CrossRef]
21. Castro, J.; Bentz, D.; Weiss, J. Effect of sample conditioning on the water absorption of concrete. *Cem. Concr. Compos.* **2011**, *33*, 805–813. [CrossRef]
22. El Mir, A.; Nehme, S.G. Porosity of Self-compacting Concrete. *Procedia Eng.* **2015**, *123*, 145–152. [CrossRef]
23. Tam, V.W.Y.; Soomro, M.; Evangelista, A.C.J. Quality improvement of recycled concrete aggregate by removal of residual mortar: A comprehensive review of approaches adopted. *Constr. Build. Mater.* **2021**, *288*, 123066. [CrossRef]
24. Ali, B.H.S.H.; Faraj, R.H.; Saeed, M.A.H.; Ahmed, H.U.; Ahmed, F.W. Innovative machine learning approaches to predict the compressive strength of recycled plastic aggregate self-compacting concrete incorporating different waste ashes. *Multiscale Multidiscip. Model. Exp. Des.* **2024**, *7*, 2585–2604. [CrossRef]
25. Rubene, S.; Vilnitis, M. Impact of low temperatures on compressive strength of concrete. *Int. J. Theor. Appl. Mech.* **2017**, *2*, 97–101.
26. Liu, Z.; Jiao, W.; Sha, A.; Gao, J.; Han, Z.; Xu, W. Portland Cement Hydration Behavior at Low Temperatures: Views from Calculation and Experimental Study. *Adv. Mater. Sci. Eng.* **2017**, *2017*, 3927106. [CrossRef]
27. Lothenbach, B.; Winnefeld, F.; Alder, C.; Wieland, E.; Lunk, P. Effect of temperature on the pore solution, microstructure and hydration products of Portland cement pastes. *Cem. Concr. Res.* **2007**, *37*, 483–491. [CrossRef]
28. Escalante-García, J.I.; Sharp, J.H. The microstructure and mechanical properties of blended cements hydrated at various temperatures. *Cem. Concr. Res.* **2001**, *31*, 695–702. [CrossRef]
29. Thomas, J.J.; Rothstein, D.; Jennings, H.M.; Christensen, B.J. Effect of hydration temperature on the solubility behavior of Ca-, S-, Al-, and Si-bearing solid phases in Portland cement pastes. *Cem. Concr. Res.* **2003**, *33*, 2037–2047. [CrossRef]
30. Almutlaqah, A.; Alshahrani, A.; Maddalena, R.; Kulasegaram, S. Performance of self-compacting concrete with treated rice husk ash at different curing temperatures. *J. Build. Eng.* **2024**, *97*, 110652. [CrossRef]
31. Hu, L.; Chen, Z.; Zhu, X.; Yang, H.; Zheng, X.; Liu, K. Effect of curing temperature on hydration and microstructure evolution of cement-based composites with extremely low w/b ratio. *Dev. Built Environ.* **2023**, *16*, 100267. [CrossRef]
32. Turcry, P.; Loukili, A.; Barcelo, L.; Casabonne, J.M. Can the maturity concept be used to separate the autogenous shrinkage and thermal deformation of a cement paste at early age? *Cem. Concr. Res.* **2002**, *32*, 1443–1450. [CrossRef]
33. Al-Shathr, B.; Abdulameer, A.; Al-Attar, T. The role of ambient temperature variation on drying shrinkage development of self-compacting Portland-limestone cement concrete. In *Proceedings of the 3rd International Conference on Buildings, Construction and Environmental Engineering, Sharm el-Shiekh, Egypt, 23–25 October 2017*; MATEC Web of Conferences: Les Ulis, France, 2018; Volume 162. [CrossRef]
34. Jiang, C.; Jin, C.; Wang, Y.; Yan, S.; Chen, D. Effect of heat curing treatment on the drying shrinkage behavior and microstructure characteristics of mortar incorporating different content ground granulated blast-furnace slag. *Constr. Build. Mater.* **2018**, *186*, 379–387. [CrossRef]
35. Lura, P.; Van Breugel, K.; Maruyama, I. Effect of curing temperature and type of cement on early-age shrinkage of high-performance concrete. *Cem. Concr. Res.* **2001**, *31*, 1867–1872. [CrossRef]

36. Almutlaqah, A.; Alshahrani, A.; Maddalena, R.; Kulasegaram, S. Enhanced fib Model Code's maturity function for strength prediction of self-compacting concrete containing supplementary cementitious materials. *Constr. Build. Mater.* **2025**, *120*, 115478. [CrossRef]
37. Muralidharan, R.; Park, T.; Yang, H.M.; Lee, S.Y.; Subbiah, K.; Lee, H.S. Review of the effects of supplementary cementitious materials and chemical additives on the physical, mechanical and durability properties of hydraulic concrete. *Materials* **2021**, *14*, 7270. [CrossRef]
38. Zhang, Z.; Zhang, B.; Yan, P. Hydration and microstructures of concrete containing raw or densified silica fume at different curing temperatures. *Constr. Build. Mater.* **2016**, *121*, 483–490. [CrossRef]
39. Xu, G.; Tian, Q.; Miao, J.; Liu, J. Early-age hydration and mechanical properties of high volume slag and fly ash concrete at different curing temperatures. *Constr. Build. Mater.* **2017**, *149*, 367–377. [CrossRef]
40. Papadakis, V.G.; Antiohos, S.; Tsimas, S. Supplementary cementing materials in concrete. *Cem. Concr. Res.* **2002**, *32*, 1533–1538. [CrossRef]
41. Lothenbach, B.; Scrivener, K.; Hooton, R.D. Supplementary cementitious materials. *Cem. Concr. Res.* **2011**, *41*, 1244–1256. [CrossRef]
42. Kadri, E.H.; Kenai, S.; Ezziane, K.; Siddique, R.; De Schutter, G. Influence of metakaolin and silica fume on the heat of hydration and compressive strength development of mortar. *Appl. Clay Sci.* **2011**, *53*, 704–708. [CrossRef]
43. Naser, M.Z.; Uppala, V.A. Properties and material models for construction materials post exposure to elevated temperatures. *Mech. Mater.* **2020**, *142*, 103293. [CrossRef]
44. Nasir, M.; Adesina, A.; Ibrahim, M.; Khan, M.U.; Baghabra Al-Amoudi, O.S.; Imran Ali, S.; Maslehuddin, M.; Saqer Alotaibi, K. Role of casting and curing conditions on the strength and drying shrinkage of greener concrete. *Environ. Sci. Pollut. Res.* **2022**, *29*, 72598–72610. [CrossRef] [PubMed]
45. EFNARC. The European Guidelines for Self-Compacting Concrete Specification, Production and Use. In *The European Guidelines for Self Compacting Concrete*; EFNARC: Flums, Switzerland, 2005.
46. *12390-3 BE*; Testing Hardened Concrete—Part 3: Compressive Strength of Test Specimens. European Committee for Standardization: Brussels, Belgium, 2003.
47. *BS EN 12390-8*; British Standard Testing Hardened Concrete. British Standard (BSI): London, UK, 2003.
48. *BS EN 12350-16*; BSI Standards Publication Testing Hardened Concrete. British Standard (BSI): London, UK, 2019.
49. *ASTM C1876*; Standard Test Method for Bulk Electrical Resistivity or Bulk Conductivity of Concrete. ASTM International: West Conshohocken, PA, USA, 2021; pp. 98–100. [CrossRef]
50. *ASTM C1585-13*; Standard Test Method for Measurement of Rate of Absorption of Water by Hydraulic Cement Concretes. ASTM International: West Conshohocken, PA, USA, 2013; Volume 41, pp. 1–6.
51. *EN 12350-12:2010*; Part 12: Self-Compacting Concrete—J-Ring Test. European Committee for Standardization: Brussels, Belgium, 2010.
52. Barkat, A.; Kenai, S.; Menadi, B.; Kadri, E.H.; Khatib, J. Relationships between Mortar Spread and the Fresh Properties of SCC Containing Local Metakaolin. *Infrastructures* **2023**, *8*, 137. [CrossRef]
53. Lu, C.; Yang, H.; Mei, G. Relationship between slump flow and rheological properties of self compacting concrete with silica fume and its permeability. *Constr. Build. Mater.* **2015**, *75*, 157–162. [CrossRef]
54. Sfikas, I.P.; Badogiannis, E.G.; Trezos, K.G. Rheology and mechanical characteristics of self-compacting concrete mixtures containing metakaolin. *Constr. Build. Mater.* **2014**, *64*, 121–129. [CrossRef]
55. Benaicha, M.; Roguiez, X.; Jalbaud, O.; Burtschell, Y.; Alaoui, A.H. Influence of silica fume and viscosity modifying agent on the mechanical and rheological behavior of self compacting concrete. *Constr. Build. Mater.* **2015**, *84*, 103–110. [CrossRef]
56. Karthik, D.; Nirmalkumar, K.; Priyadharshini, R. Characteristic assessment of self-compacting concrete with supplementary cementitious materials. *Constr. Build. Mater.* **2021**, *297*, 123845. [CrossRef]
57. Al-Oran, A.A.A.; Safiee, N.A.; Nasir, N.A.M. Fresh and hardened properties of self-compacting concrete using metakaolin and GGBS as cement replacement. *Eur. J. Environ. Civ. Eng.* **2022**, *26*, 379–392. [CrossRef]
58. Liu, M. Self-compacting concrete with different levels of pulverized fuel ash. *Constr. Build. Mater.* **2010**, *24*, 1245–1252. [CrossRef]
59. Tahmid, A.; Chowdhury, S.R.; Tonmoy, F.F.; Moon, T.K. Analyzing the Filling Ability Property of Self-Compacting Concrete Using Fly Ash and Superplasticizer. *J. Civ. Constr. Eng.* **2021**, *7*, 23–32. [CrossRef]
60. Shrihari, S.; Seshagiri Rao, M.V.; Srinivasa Reddy, V. Evaluation of Cementing Efficiency of Quaternary Blended High Strength Self Compacting Concrete. *Int. J. Res. Eng. Technol.* **2016**, *05*, 260–265. [CrossRef]
61. Gesoğlu, M.; Güneyisi, E.; Özbay, E. Properties of self-compacting concretes made with binary, ternary, and quaternary cementitious blends of fly ash, blast furnace slag, and silica fume. *Constr. Build. Mater.* **2009**, *23*, 1847–1854. [CrossRef]
62. Gajewicz-Jaromin, A.M.; McDonald, P.J.; Muller, A.C.A.; Scrivener, K.L. Influence of curing temperature on cement paste microstructure measured by 1H NMR relaxometry. *Cem. Concr. Res.* **2019**, *122*, 147–156. [CrossRef]

63. Li, L.; Feng, T.; Li, Y.; Zhang, Y.; Sun, W.; Liu, Z. Evaluating the effect of high fly ash content and low curing temperature on early hydration heat of blended cement based on isothermal calorimetric method. *Constr. Build. Mater.* **2024**, *430*, 136110. [CrossRef]
64. Khatib, J.M. Low Temperature Curing of Metakaolin Concrete. *J. Mater. Civ. Eng.* **2009**, *21*, 362–367. [CrossRef]
65. Yousuf, S.; Shafigh, P.; Ibrahim, Z.; Hashim, H.; Panjehpour, M. Crossover effect in cement-based materials: A review. *Appl. Sci.* **2019**, *9*, 2776. [CrossRef]
66. Gonzalez-Corominas, A.; Etxeberria, M.; Poon, C.S. Influence of steam curing on the pore structures and mechanical properties of fly-ash high performance concrete prepared with recycled aggregates. *Cem. Concr. Compos.* **2016**, *71*, 77–84. [CrossRef]
67. Liu, J.; Li, Y.; Ouyang, P.; Yang, Y. Hydration of the silica fume-Portland cement binary system at lower temperature. *Constr. Build. Mater.* **2015**, *93*, 919–925. [CrossRef]
68. Chen, L.; Zheng, K.; Xia, T.; Long, G. Mechanical property, sorptivity and microstructure of steam-cured concrete incorporated with the combination of metakaolin-limestone. *Case Stud. Constr. Mater.* **2019**, *11*, e00267. [CrossRef]
69. Cano Barrita Fde, J.; Bremner, T.W.; Balcom, B.J. Effects of curing temperature on moisture distribution, drying and water absorption in self-compacting concrete. *Mag. Concr. Res.* **2003**, *55*, 517–524. [CrossRef]
70. Güneyisi, E.; Gesoğlu, M.; Karaoğlu, S.; Mermerdaş, K. Strength, permeability and shrinkage cracking of silica fume and metakaolin concretes. *Constr. Build. Mater.* **2012**, *34*, 120–130. [CrossRef]
71. Leung, H.Y.; Kim, J.; Nadeem, A.; Jaganathan, J.; Anwar, M.P. Sorptivity of self-compacting concrete containing fly ash and silica fume. *Constr. Build. Mater.* **2016**, *113*, 369–375. [CrossRef]
72. Liu, B.; Luo, G.; Xie, Y. Effect of curing conditions on the permeability of concrete with high volume mineral admixtures. *Constr. Build. Mater.* **2018**, *167*, 359–371. [CrossRef]
73. Chahal, N.; Siddique, R.; Rajor, A. Influence of bacteria on the compressive strength, water absorption and rapid chloride permeability of concrete incorporating silica fume. *Constr. Build. Mater.* **2012**, *37*, 645–651. [CrossRef]
74. Morsy, M.S. Effect of temperature on hydration kinetics and stability of hydration phases of metakaolin-lime sludge-silica fume system. *Ceram.—Silik.* **2005**, *49*, 237–241.
75. Liu, Y.; Presuel-Moreno, F.J. Normalization of temperature effect on concrete resistivity by method using Arrhenius law. *ACI Mater. J.* **2014**, *111*, 433–442. [CrossRef]
76. Utkan, Ç.; Kesler, E.; Yıkıcı, T.A.; Akkaya, Y. Effects of curing temperature on chloride migration and electrical resistivity of concrete. In *Proceedings of the Conference on Materials, Systems and Structures in Civil Engineering, Lyngby, Denmark, 15–29 August 2016*; RILEM Publications: Bagneux, France, 2016.
77. Gallucci, E.; Zhang, X.; Scrivener, K.L. Effect of temperature on the microstructure of calcium silicate hydrate (C-S-H). *Cem. Concr. Res.* **2013**, *53*, 185–195. [CrossRef]
78. Liu, J.; Li, Y.; Yang, Y.; Cui, Y. Effect of low temperature on hydration performance of the complex binder of silica fume-portland cement. *J. Wuhan Univ. Technol. Mater. Sci. Ed.* **2014**, *29*, 75–81. [CrossRef]
79. Siddique, R.; Khan, M.I. *Supplementary Cementing Materials*; Springer: Berlin/Heidelberg, Germany, 2011; pp. 67–119. [CrossRef]
80. Jiang, C.; Yang, Y.; Wang, Y.; Zhou, Y.; Ma, C. Autogenous shrinkage of high performance concrete containing mineral admixtures under different curing temperatures. *Constr. Build. Mater.* **2014**, *61*, 260–269. [CrossRef]
81. Maruyama, I.; Teramoto, A. Temperature dependence of autogenous shrinkage of silica fume cement pastes with a very low water–binder ratio. *Cem. Concr. Res.* **2013**, *50*, 41–50. [CrossRef]
82. Klausen, A.E.; Kanstad, T.; Bjøntegaard, Ø.; Sellevold, E.J. The effect of curing temperature on autogenous deformation of fly ash concretes. *Cem. Concr. Compos.* **2020**, *109*, 103574. [CrossRef]
83. Thomas, J.J.; Jennings, H.M. Effect of heat treatment on the pore structure and drying shrinkage behavior of hydrated cement paste. *J. Am. Ceram. Soc.* **2002**, *85*, 2293–2298. [CrossRef]
84. Wang, L.; Yu, Z.; Liu, B.; Zhao, F.; Tang, S.; Jin, M. Effects of Fly Ash Dosage on Shrinkage, Crack Resistance and Fractal Characteristics of Face Slab Concrete. *Fractal Fract.* **2022**, *6*, 335. [CrossRef]